

Symposium-in Print

Phantoms for Noninvasive Blood Glucose Sensing with Near Infrared Transmission Spectroscopy

Jason J. Burmeister, Hoell Chung* and Mark A. Arnold†

Department of Chemistry, University of Iowa, Iowa City, IA, USA

Received 15 April 1997; accepted 5 September 1997

ABSTRACT

In vivo spectra from human subjects can be simulated with a phantom composed of different layers of water, fat and muscle tissue. All three components are necessary to simulate *in vivo* spectra collected over the combination spectral region (5000–4000 cm^{-1}). Muscle tissue is not required, however, to accurately simulate overtone spectra (6600–5400 cm^{-1}). The near-IR spectral characteristics of fat and muscle tissue from several animal sources are essentially identical to those found for human tissue, hence, the animal source for these phantom components is not critical. Thickness of each tissue layer can be determined by a regression analysis where the *in vivo* spectrum of interest is regressed against standard absorbance spectra of the necessary model components (water, fat and muscle). In general, *in vivo* overtone spectra collected across human webbing tissue with a thickness of 6.7 mm can be simulated with water layer thicknesses ranging from 5.0 to 6.4 mm combined with fat layer thicknesses from 1.4 to 4.2 mm.

INTRODUCTION

Near infrared (NIR)‡ spectroscopy is proposed as a method for measuring blood glucose levels within the human body in a noninvasive and painless manner. The idea is to pass a band of NIR radiation through a vascular region of the body and then extract the analytical information from the resulting spectral information. Success of this approach demands high-quality spectra combined with sophisticated data processing. The NIR spectra collected from human subjects must possess sufficient signal-to-noise to permit reliable differentiation of the small glucose absorbance signals relative to the underlying spectral noise. Sophisticated data-processing tools are needed to enhance selectivity by distinguishing

glucose absorbance features from those for other molecular species in the sample matrix.

Our approach to assessing the utility of NIR spectroscopy for measuring blood glucose noninvasively is to begin with glucose measurements in relatively simple matrices and then increase the matrix complexity with the ultimate goal of the human body. We started with glucose in a simple aqueous phosphate buffer (1) before examining more complex matrices (2–4) that contained potential interferences such as proteins, triglycerides, amino acids, *etc.* Regardless of the matrix complexity, valid glucose calibration models have been successfully developed from the NIR spectral information.

A phantom is required to effectively extend our development of NIR spectroscopy for noninvasive blood glucose sensing from aqueous solutions to the human body. Sequential layers of fatty tissue and aqueous buffer are proposed as a phantom to simulate NIR transmission spectra of human tissue. This phantom provides a means for collecting NIR spectra under *in vitro* conditions that accurately simulate *in vivo* spectra. Such a phantom permits control of critical experimental parameters, thereby facilitating method development. The effectiveness of such phantoms has been demonstrated in studies to explore the potential of NIR for measuring hemoglobin and imaging tumors in tissue matrices (5–7).

EXPERIMENTAL

Instrumentation. Spectra were collected with a Nicolet 740 Fourier transform spectrometer equipped for measurements in the near infrared. Specifically, this spectrometer was equipped with a 400 W tungsten-halogen lamp source, calcium fluoride beam splitter and cryogenically cooled InSb detector for the combination region and a thermoelectrically cooled InGaAs detector for the overtone region (8). Interference filters were used to isolate either the combination or overtone region, respectively.

Tissue samples. Skin, muscle and fat tissue samples were dissected from various animals. Chicken, porcine and bovine samples were purchased from a local grocery store. Dog, sheep and rat tissues were obtained from the Animal Research Center at the University of Iowa by an approved protocol. Human tissue samples were obtained from the University of Iowa Hospitals and Clinics by a protocol approved by the Human Subjects Internal Review Board on campus. All samples were stored at 4°C.

Animal tissue samples were dissected to isolate the fat, skin and muscle layers. These layers were then individually positioned be-

*Present address: Yukong, Ltd., Ulsan Research Center, Chemical Process Research Laboratory, Ulsan, Korea.

†To whom correspondence should be addressed at Department of Chemistry, University of Iowa, Iowa City, IA 52242; USA. Fax: 319-353-1115; e-mail: mark-arnold@uiowa.edu

‡Abbreviations: NIR, near infrared; RMS, root mean square.

© 1998 American Society for Photobiology 0031-8655/98 \$5.00+0.00

(

e

f

e

(

s

a

(

tween two 25.4 mm diameter sapphire windows and gently squeezed to reach the desired thickness. Tissue thickness was 1 mm for all measurements in the combination region. Tissue thickness varied, as specified below, for measurements in the overtone region. Care was taken to avoid trapping air bubbles within the tissue matrix that would adversely affect the spectroscopy by transmitting unattenuated incident radiation. Each sandwiched tissue sample was positioned in a temperature-controlled cell mount (Wilnad model 118) within the spectrometer for data collection.

Phantoms were constructed by combining layers of blended beef fat and an aqueous phosphate buffer (0.1 M, pH 7.35). The beef fat was placed between two 25.4 mm sapphire windows with a Teflon spacer ring to control the fat layer thickness. Once assembled, silicone rubber cement was used to hold the windows together. The resulting fat filters were durable and easy to handle. The aqueous layer was held in a conventional temperature controlled variable pathlength sample holder (Wilnad model 118). Spectra were collected after mounting each component in the sample compartment of the spectrometer. The aqueous layer was placed in the normal sample holder at the focal point of the incident beam. A 25.4 mm diameter convex lens (33 mm focal length) was mounted in front of the aqueous layer and the fat filter was mounted before this lens. This position for the fat filter was most convenient experimentally and filter position had no significant impact on spectral quality.

The webbing between the thumb and forefinger served as the measurement site for *in vivo* human spectra. Webbing spectra were collected by pinching a section of the webbing between a set of sapphire windows. The sandwiched webbing tissue was held in the sample compartment of the spectrometer with the webbing positioned at the focal point of the incident beam. For the combination region a 25.4 mm diameter, 33 mm focal length, convex lens was used to focus the incident light on the webbing. No temperature control was attempted.

Spectra. The NIR spectra were collected as 256 co-added, double-sided, 16k interferograms that were subsequently transformed to single beam spectra with 1.9 cm^{-1} point spacing. Before collecting each spectrum, the sample was heated to 37°C. Wire screens of various mesh sizes were used to attenuate the incident light intensity as needed to avoid saturating the detector and to match intensity levels between sample and background spectra. Air background spectra were collected with the same instrument settings, and absorbances were computed accordingly. All single-beam spectra were transferred to an Iris Indigo computer (Silicon Graphics, Inc.) for processing with software provided by Professor Gary W. Small from the Center of Intelligent Chemical Instrumentation in the Department of Chemistry at Ohio University (Athens, OH). Regression analyses were performed with either Minitab (release 8) or Sigma Plot for DOS on a common desktop computer.

RESULTS AND DISCUSSION

In vivo human spectra

The NIR spectra were collected over both the combination and overtone regions. The combination region is located between 5000 and 4000 cm^{-1} (2.0–2.5 μm) and the first overtone region is located between 6500 and 5400 cm^{-1} (1.54–1.85 μm). In general, the combination region offers larger absorptivities and sharper spectral features that result in superior analytical performance. Unfortunately, strong water absorption in the combination region limits sample thickness to 1–2 mm. In comparison, sample path lengths as large as 10 mm can be easily accommodated in the overtone region where water absorptivity is significantly lower. These offsetting characteristics make each of these spectral regions worthy of investigation.

In vivo human spectra possess similar absorbance features regardless of the spectral range. Single-beam spectra are presented in Fig. 1 for both the combination and overtone regions. The webbing tissue was squeezed to a thickness of 2.5 mm for the combination region, while the tissue thick-

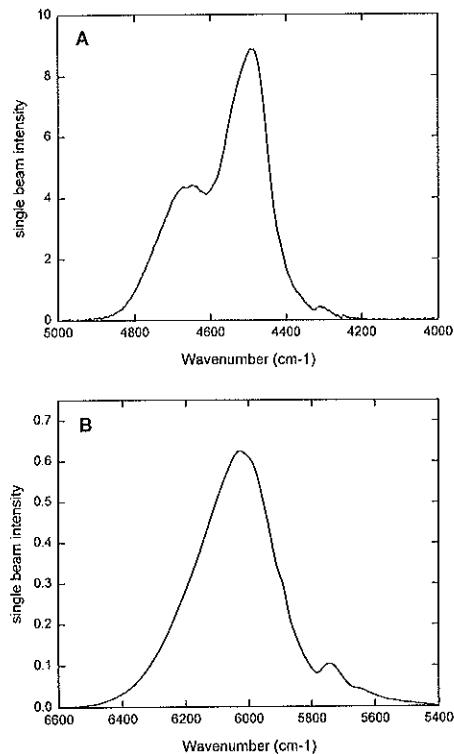


Figure 1. *In vivo* single-beam spectra collected through human webbing tissue over the combination (A) and overtone (B) spectral regions.

ness was 6.7 mm for the overtone spectrum. In both cases, light transmission is greatly attenuated at both the high- and low-frequency extremes with the greatest transmission in the center portion of the spectrum. As will be shown below, water is primarily responsible for attenuating the high-frequency radiation and fatty tissue attenuates the low-frequency light. The combination spectrum possesses an absorbance feature around 4600 cm^{-1} and a sharp drop in transmitted light around 4475 cm^{-1} . The overtone spectrum, on the other hand, has a broader transmission window with fewer absorbance features.

Animal tissue models for combination spectra

The NIR spectral characteristics of fat, skin, and muscle were evaluated as possible phantom components for *in vivo* human spectra.

Initially, spectra were collected for chicken fat, skin and muscle over the combination region. The resulting single-beam spectra are presented in Fig. 2 along with a single-beam spectrum for water. Fat is characterized by two strong absorption bands centered at 4350 and 4270 cm^{-1} . These absorbances are sufficiently broad and strong that little light is transmitted beyond 4400 cm^{-1} with the sharp drop in transmission beginning around 4475 cm^{-1} . This fatty tissue corresponds to adipose tissue that contains dense clusters of large fat storage cells (9). These strong absorbances are likely caused by the combinations of C–H vibrational transitions associated with the long alkyl chains of the fat molecules. Skin possesses essentially the same spectral features as fat, but smaller in magnitude. This finding suggests that fatty

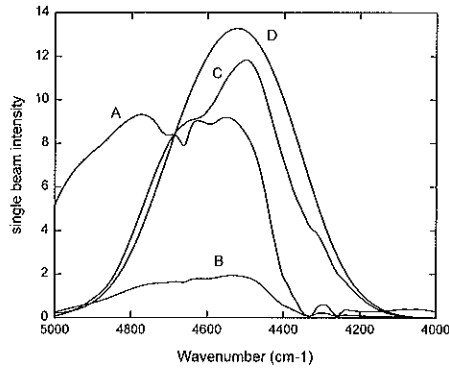


Figure 2. Single-beam combination spectra for isolated pieces of chicken fat (A), chicken skin (B), chicken muscle (C) and phosphate buffer (D).

tissue within the skin matrix is primarily responsible for its NIR spectral features. The NIR spectrum of muscle tissue is similar to that for water with additional absorption features around 4600 and 4370 cm^{-1} . Like water, muscle strongly attenuates light at both high and low frequency extremes. The additional features at 4600 and 4370 cm^{-1} correspond to protein that is known to possess strong absorption features at these locations (10). Water and muscle both allow maximum transmission of light between 4600 and 4400 cm^{-1} . The resemblance between muscle and water is reasonable considering the high water content of muscle tissue (*ca* 75–85%) (11).

Interspecies variation was assessed by comparing absorbance spectra collected from fat and muscle samples obtained from human, chicken, bovine, porcine, hamster, dog and sheep sources. The NIR spectra from these fat samples revealed the exact same absorbance features regardless of the animal source. Likewise, all muscle absorbance spectra were essentially identical. Although the absorptivities may differ between species, the position and widths of the absorbance bands were indistinguishable. These spectral similarities are expected given the chemical uniformity of fat and muscle tissue and the limited chemical sensitivity of NIR spectroscopy. Chemically, all fatty tissue is principally composed of CH_2 groups which dominates the NIR spectra. From a practical standpoint, these findings suggest that the source of tissue is not important when designing the proposed phantom.

Comparison of the combination spectra shown in Fig. 2 for the various tissue materials and the corresponding *in vivo* human spectrum shown in Fig. 1A reveals that the principle components of the *in vivo* spectrum are water, muscle and fat. Water and muscle combine to dictate the spectral features at wavenumbers greater than 4500 cm^{-1} while fat absorption dictates the spectrum at wavenumbers below 4500 cm^{-1} . Hence, *in vivo* spectra from human subjects can be simulated by using combinations of these tissue materials.

Magnitude of the fat absorbance bands can be varied by altering the amount of fatty tissue placed in the optical path. Figure 3 shows this effect with a series of absorbance spectra for different amounts of bovine fat. Larger absorbances are observed as more fat tissue is packed between the optical windows, thereby increasing the packing density of material in the optical beam. Increasing absorbance is clearly evident

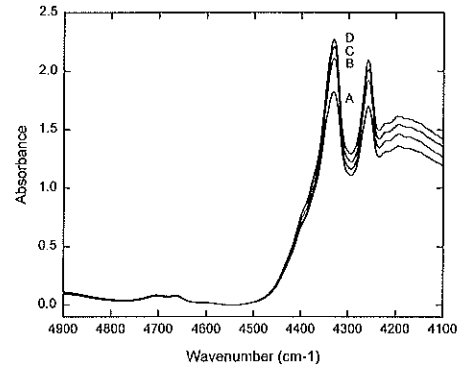


Figure 3. Absorbance spectra for beef fat densities (g/cm^3) of 1.05 (A), 1.28 (B), 1.50 (C) and 1.71 (D).

at the lower frequencies and these increases in absorbance help to better define the fat absorbance features. Such behavior is critical for the proposed phantom because different amounts of body fat can be simulated by simply controlling the amount of fat in the phantom.

The position of many NIR absorption bands is notoriously sensitive to temperature, which can dramatically degrade analytical performance. The temperature sensitivity for the fatty tissue has been examined to determine the extent to which temperature control will be needed when used in the phantom. Absorbance spectra for fat at 20.3 and 37.1°C are provided in Fig. 4 for comparison. Although these bands shift to higher frequency at the higher temperature, this shift is slight given the large temperature difference (*ca* 0.2 $\text{cm}^{-1}/^\circ\text{C}$). Such a small temperature coefficient suggests rigorous temperature control is not necessary for the fat layer. Magnitude of the extinction coefficient, however, is more sensitive to temperature, particularly around the melting point. For this reason, large temperature variations should be avoided.

In vitro phantoms for overtone spectra

Examination of overtone spectra collected from isolated samples of fat and muscle samples led to the same conclusions as noted above for combination spectra. Overtone spectra for each tissue type are essentially identical regardless of the animal source. Again, fat absorbance dominates at low frequencies while water strongly attenuates the high-

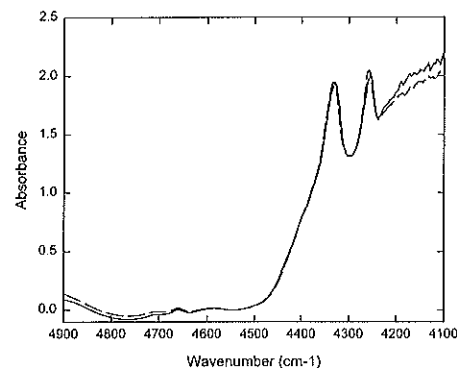


Figure 4. Absorbance spectra for beef fat collected at 20.3°C (solid line) and 37.1°C (dashed line).

Table 1. Results for phantoms fitted by the three-layer model (water/fat/muscle)

Webbing	β_0^*	β_1^*	β_2^*	β_3^*	l_{water}^\dagger	l_{fat}^\dagger	$l_{\text{muscle}}^\dagger$	RMS‡
1	-1.51	1.16	0.964	2.45	4.77	1.66	1.57	0.06652
2	0.417	1.28	1.89	0.618	5.26	3.25	0.40	0.05869
3	0.364	1.36	1.39	0.648	5.59	2.39	0.41	0.04969
4	0.679	1.32	2.45	-0.0807	5.43	4.21	-0.052	0.06603
5	-0.086	1.07	1.24	2.17	4.40	2.13	1.39	0.05145
6	0.766	1.29	1.35	0.431	5.30	2.32	0.28	0.04742
7	1.29	1.37	2.30	-1.02	5.63	3.96	-0.65	0.07093

*Regression coefficients.

†Modeled tissue thickness (mm).

‡Root mean square for model residuals.

frequency radiation. As is detailed below, protein absorption is less significant in the overtone region compared to the combination region. Hence, a layer of muscle is not required to provide a suitable phantom for overtone spectra.

An effective phantom must provide *in vitro* spectra that match *in vivo* spectra in terms of position and magnitude of all absorption features. If successfully matched, the transmission properties of the phantom will closely resemble those of living human tissue. The key to success is to find the proper relative thicknesses of the model components.

A regression method is proposed to identify the best combination of tissue thicknesses to accurately simulate human *in vivo* spectra. In this technique, absorbance spectra from pure samples of water, beef fat and beef muscle are combined according to the following expression:

$$S_H = \beta_0 + \beta_1 S_w + \beta_2 S_f + \beta_3 S_m$$

where S_H , S_w , S_f and S_m correspond to absorbance spectra for known thicknesses of human webbing, water, beef fat and beef muscle, respectively, and β_i corresponds to the respective regression coefficient. Absorbance spectra are used because of the additive nature of Beer's law. In this method, a given *in vivo* human webbing spectrum is fit by combining the individual tissue absorbance spectra. The best relative amount of each tissue spectrum is given by the regression coefficients. The best absolute amount of each tissue can then be computed as the product of the regression coefficient and the tissue thickness used to collect the standard absorbance spectrum for the individual tissue components. In addition, β_0 corresponds to the total optical throughput of the

sample and is heavily influenced by tissue-scattering processes.

In vivo human webbing spectra from seven different volunteers were modeled to evaluate the utility of the proposed regression technique. The *in vivo* spectra were collected through 6.73 mm of webbing tissue from seven healthy individuals. Spectra were also collected for individual samples of phosphate buffer (pH 7.35, 4.1 mm thick), beef fat (1.7 mm thick) and beef muscle (0.6 mm thick). Absorbance spectra were then computed by using an appropriately matched air background spectrum. Human webbing spectra were then regressed relative to the standard spectra over the entire spectral range (6600–5400 cm^{-1}). This regression analysis was performed twice for each webbing spectrum. The term for muscle ($\beta_3 S_m$) was included the first time and removed the second. Results from both regression analyses are presented in Tables 1 and 2.

Fitted spectra compare favorably to the corresponding *in vivo* spectra. Figure 5 provides an example where two fitted spectra are superimposed on the corresponding *in vivo* spectrum. In the first case, all three phantom components, water, fat and muscle, were used to generate this fitted spectrum. In the second case, only water and fat layers were considered. Although the match is not exact in either case, both fitted spectra clearly follow the general trend of the *in vivo* spectrum. These fitted spectra match the actual spectrum over much of the spectral range. The major deviation between fitted and actual spectra occurs at the high-frequency fat absorbance band. For most spectra tested, fitted spectra

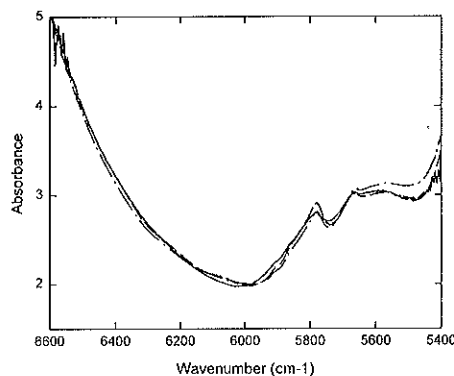
Table 2. Results for phantoms fitted by the two-layer model (water/fat)

Webbing	β_0^*	β_1^*	β_2^*	l_{water}^\dagger	l_{fat}^\dagger	RMS‡
1	-0.0968	1.53	0.799	6.29	1.37	0.1032
2	0.775	1.38	1.85	5.67	3.18	0.06503
3	0.739	1.46	1.35	6.00	2.32	0.05460
4	0.632	1.30	2.46	5.34	4.23	0.06569
5	1.17	1.39	1.10	5.71	1.89	0.08711
6	1.02	1.35	1.32	5.55	2.27	0.04919
7	0.698	1.22	2.37	5.01	4.08	0.07827

*Regression coefficients.

†Modeled tissue thickness (mm).

‡Root mean square for model residuals.

**Figure 5.** *In vivo* absorbance spectrum of human webbing (solid line) and the corresponding fitted spectra with the water/fat/muscle model (dashed line) and the water/fat model (dashed-dot line).

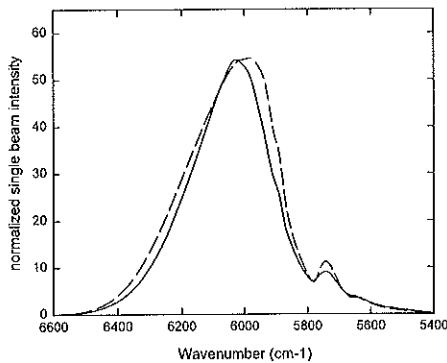


Figure 6. Single-beam spectra for a human webbing (solid line) and the corresponding water/fat phantom (dashed line).

consistently overestimate the magnitude of absorbance for this band. Quality of the match was quantified by computing the root mean square (RMS) of the residuals between real and fitted spectra. The RMS of the residuals are 0.067 and 0.103, respectively, for the three- and two-component fitted spectra shown in Fig. 5.

Muscle has little impact on the regression results. The mean of the residuals for all seven *in vivo* spectra fitted with water, fat and muscle is 0.059. When only water and fat are used, the mean RMS of the residuals is 0.072. Also, the two fitted spectra shown in Fig. 5 are similar, particularly for the water region. The presence or absence of muscle in the model only affects the first regression coefficient (β_0). This term is sensitive to the total light throughput and therefore corresponds to various optical properties of the system including source power, detectivity of the detector, scattering properties of the sample, *etc.* A layer of muscle tissue scatters some of the incident radiation that alters the optical throughput, thereby changing the magnitude of β_0 . The absence of a strong protein absorption band in the *in vivo* spectra permits excluding muscle in the phantom.

The regression analysis provides the information needed to construct a phantom to simulate a given *in vivo* spectrum. The spectrum fitted with two components in Fig. 5, for example, predicts that a phantom composed of a 6.3 mm thick layer of phosphate buffer and 1.4 mm thick layer of fat will best simulate the *in vivo* spectrum. A phantom composed of 6.2 mm buffer and 1.6 mm fat was constructed and spectrum collected. The resulting single-beam spectrum from the phantom is presented in Fig. 6 along with the corresponding *in vivo* single-beam spectrum. Overall, the phantom spectrum in Fig. 6 compares favorably with the targeted *in vivo* spectrum that validates the regression method and supports the use of the proposed phantom to simulate noninvasive experiments.

Potential Applications. The proposed *in vitro* model offers a means to generate single beam spectra that accurately simulate spectra collected noninvasively. The ability to simulate single-beam spectra is critical because future attempts to develop noninvasive NIR spectroscopic clinical methods will likely rely upon the analysis of single-beam spectra. As detailed elsewhere [12], the generation of absorbance spectra is complicated by severe mismatch between the sample matrix and putative background materials. Fortunately, accurate glucose predictions are possible from PLS calibration mod-

els generated from single-beam spectra [12]. In fact, essentially identical model performance is obtained with single-beam and ratioed spectra. Alternatively, the proposed phantom may serve as an acceptable reference material from which suitable background spectra can be obtained.

In addition, the proposed model offers the ability to vary the thickness of the aqueous and fat layers, thereby providing in mechanism for simulating different *in vivo* measurement conditions. Proper control of layer thickness is necessary to simulate different measurement sites, such as ear lobes or fingers, where the relative amounts of water, fat and muscle will likely be much different than the webbing tissue examined here. Furthermore, the composition of a given measurement site will vary between individuals and within a given individual with time. The proposed phantom can accommodate such experimental variation by appropriate adjustment of layer thickness.

CONCLUSIONS

The proposed tissue phantom will greatly facilitate the development of NIR spectroscopy for noninvasive clinical measurements. This *in vitro* model offers a mechanism for controlling critical experimental parameters, thereby providing a means for reproducible conditions. The level of reproducibility promised by this phantom is impossible to achieve with actual human subjects. The effect of optical path length can be examined by varying the aqueous layer thickness. Interference from fatty tissue can be documented by using different fat layer thicknesses. Finally, light-scattering effects can be determined by adding scattering particles to the aqueous layer. The phantom allows each of these demanding experiments to be performed in a rigorous and systematic manner.

Acknowledgements—This work was supported by a grant from the National Institute of Diabetes and Digestive and Kidney Diseases (DK45126). We thank Kevin H. Hazen whose instrumental modifications allowed the high spectral quality seen in this work.

REFERENCES

1. Arnold, M. A. and G. W. Small (1990) Determination of physiological levels of glucose in an aqueous matrix with digitally filtered Fourier transform near-infrared spectra. *Anal. Chem.* **62**, (1990) 1457–1464.
2. Chung, H., M. A. Arnold, M. Rhiel and D. W. Murhammer (1996) Simultaneous measurements of glucose, glutamine, ammonia, lactate and glutamate in aqueous solutions by near-infrared spectroscopy. *Appl. Spectrosc.* **50**, 270–276.
3. Chung, H., M. A. Arnold, M. Rhiel and D. W. Murhammer (1995) Simultaneous measurement of glucose and glutamine in aqueous solutions by near infrared spectroscopy. *Appl. Biochem. Biotechnol.* **50**, 109–126.
4. Marquardt, L. A., M. A. Arnold and G. W. Small (1993) Near infrared spectroscopic measurement of glucose in a protein matrix. *Anal. Chem.* **65**, 3271–3278.
5. Franceschini, M. A., S. Fantini, A. Cerussi, B. Barbieri, B. Chance and E. Gratton (1996) The effect of scatter in quantitation of hemoglobin concentration in a tissue-like phantom by near-infrared spectroscopy. In *Biomedical Spectroscopy and Diagnostics*, 1996 Technical Digest, pp. 27–29. Optical Society of America, Washington, DC.
6. Sevich-Muraca, E. M. (1996) Optical properties of normal and diseased breast tissues: prognosis for optical mammography. *J. Biomed. Opt.* **3**, 342–355.
7. Patterson, M., S. Andersson-Engels, B. Wilson and E. Osei (1995) Absorption spectroscopy in tissue-simulating materials:

- a theoretical and experimental study of photon paths. *Appl. Opt.* **34**, 22–30.
8. Hazen, K. H. (1995) Glucose determination in biological matrices using near-infrared spectroscopy, Ph.D. Dissertation, University of Iowa, Iowa City.
 9. Starr, C. and R. Taggart (1987) *Biology, The Unity and Diversity of Life*, 4th ed. Wadsworth, Belmont, CA.
 10. Pan, S., Chung, M. A. Arnold and G. W. Small (1996) Near-infrared spectroscopic measurement of physiological glucose levels in variable matrices of protein and triglycerides. *Anal. Chem.* **68**, 1124–1135.
 11. Starr and R. Taggart (1987) *Biology, The Unity and Diversity of Life*, 4th ed. Wadsworth, Belmont, CA.
 12. Lu, G., X. Zhou, M. A. Arnold and G. W. Small (1997) Multivariate calibration models based on the direct analysis of near-infrared spectra. *Appl. Spectrosc.* **51**, no. 9, 1330–1339.

(

1
1
4

(

1
1
1

(